UCRL-JC-141689
PREPRINT

Reduction of Stimulated Scattering Losses from Hohlraum Plasmas with Laser Beam Smoothing

S.H. Glenzer, R.L. Berger, L.M. Divol, R.K. Kirkwood, B.J. MacGowan, J.D. Moody, J.E. Rothenberg, L.J. Suter, and E.A. Williams

This paper was prepared for submittal to
Physics of Plasma

November 2000

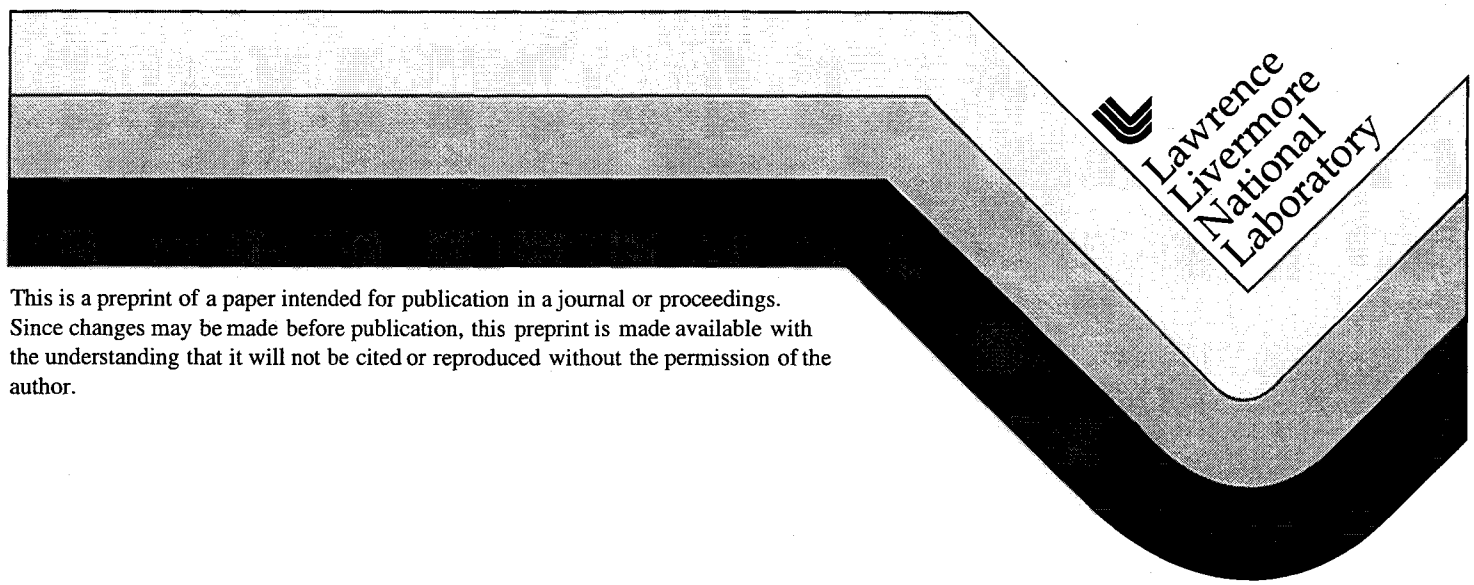

Reduction of stimulated scattering losses from Hohlraum Plasmas with Laser Beam Smoothing

S. H. Glenzer, R. L. Berger, L. M. Divol*, R. K. Kirkwood, B. J. MacGowan, J. D. Moody, A. B. Langdon, L. J. Suter, and E. A. Williams

Lawrence Livermore National Laboratory, University of California P. O. Box 808, CA 94551, U.S.A.

* *CEA/DIF/DCSA/SET BP 12, 91680 Bruyères-Le-Châtel, France*

Abstract

Laser beam smoothing by spectral dispersion and by polarization smoothing has been observed to significantly reduce the scattering losses by stimulated Brillouin and stimulated Raman scattering from inertial confinement fusion hohlraums. For these measurements, the laser beam smoothing and the high−Z hohlraum wall plasma parameters approach the conditions of future inertial confinement fusion experiments. The simultaneous application of the smoothing techniques has reduced the scattering losses by almost one order of magnitude down to the 1 % level. The experimental scaling of the stimulated Brillouin reflectivity compares well to modeling assuming nonlinear damping on the ion acoustic waves in three dimensional non-linear wave simulations and calculated hohlraum plasma conditions from radiation-hydrodynamic modeling.

PACS numbers: 52.35 Fp, 52.58 Ns, 52.25 Rv, 52.40 Nk, 52.50 Jm, 52.70 Kz

I. INTRODUCTION

To optimize laser-target coupling in laser-driven inertial confinement fusion (ICF) research, it is essential to control and suppress laser scattering losses by stimulated Brillouin (SBS) and stimulated Raman (SRS) scattering[1–5]. These processes are parametric decay instabilities where an incident light wave decays into an ion acoustic wave (electron plasma wave) and a scattered electromagnetic wave in case of SBS (SRS). These instabilities grow in the long scale-length coronal plasmas that are produced by the interaction of high-energy several nanoseconds long laser pulses with matter. Suppressing the laser light losses due to SBS and SRS by reducing the fraction of high-intensity hot spots in the laser beam with laser beam smoothing is important for the success of ICF.

In the indirect drive approach to ICF, the fusion capsule is contained in a gas-filled hohlraum. In the high$-Z$ wall plasma of the hohlraum, laser light is converted into soft x rays that produce a homogeneous x-ray ablation pressure on the capsule surface to achieve a high-convergence, high-yield implosion. The (cryogenic) low$-Z$ gas fill slows down the high$-Z$ blow-off plasma from the hohlraum walls which is important for controlling the symmetry of the capsule implosion. The gas fill turns into a long-scale length plasma where SRS is the dominant instability while SBS grows preferentially in the high$-Z$ wall plasma because of the high density, weak velocity gradients, and small ion wave damping. In addition to the reduced soft x-ray production in the hohlraum[6], SBS and SRS may affect the implosion symmetry, cause laser damage and capsule pre-heat. For these reasons, it is essential to test laser beam smoothing techniques for the suppression of SBS and SRS.

In this study, laser-plasma interaction experiments have been performed in ICF hohlraums with laser beam conditions almost identical to the design of future ICF experiments, e.g. at the National Ignition Facility (NIF). For this purpose, the scattered light by SBS and SRS has been measured on one f/8 interaction beam that has operated at 3ω (351.1 nm) and focussed into gas-filled hohlraums. Due to the 1 atm methane (CH_4) gas fill, the conditions in the Au blow off plasma are close to those calculated for NIF hohlraums.

The SBS interaction is limited in both these experiments and in NIF to the light absorption length in the gold plasma which is independent of the hohlraum size. The effects of several beam smoothing techniques have been tested including random phase plates, laser beam smoothing by spectral dispersion (SSD)[7] and polarization smoothing (PS)[8–10]. A high-frequency modulator of 17 GHz has been applied consistent with the NIF architecture. The application of PS together with 17 GHz SSD, with fewer independent speckle patterns than previous SSD experiments with 3 GHz, e.g.[5,11], is an important new test of ICF beam smoothing schemes.

The experiments show that SSD is effective in reducing the scattering losses due to SBS and SRS by about one order of magnitude for the NIF-like laser intensity of 2×10^{15}W cm^{-2} as well as for a higher intensity of 4×10^{15}W cm^{-2}. Polarization smoothing further reduces the scattering levels and is clearly beneficial for high laser intensities indicating that high radiation temperature hohlraums may be accessible with the NIF.

We have also extensively modeled the laser-plasma interactions in gas-filled hohlraums and compared the calculated with experimental SBS reflectivities for the various laser beam smoothing conditions. These calculations use the codes LIP and F3D. In LIP, the gain exponent[12] of the backscattered SRS and SBS light is calculated along a path through the LASNEX-generated plasma profile as a function of the scattered light frequency with the effects of inhomogeneity and multiple-ion species included. The mean intensity along the path is calculated from the (time-dependent) incident power given the focal length, f-number, and the inverse bremsstrahlung absorption rate. No account of self-focusing, beam smoothing or pump depletion is taken. In the calculations shown in this report, the spectrum did not include the instrumental broadening. In F3D[13] the incident laser and reflected light propagate within the paraxial approximation and drive ion acoustic waves by ponderomotive forces that backscatter, self-focus, and forward Brillouin scatter the light. The non-linear saturation mechanisms and other physics in F3D have been described in detail Ref.[13]. Because the hohlraum plasma conditions show very small calculated gain values for SRS consistent with the time-integrated SRS losses of ≤ 1 % for almost all laser

beam smoothing conditions, we only compare the F3D modeling to the SBS instability. The F3D modeling consistently predicts negligible SRS in the gold blow-off plasma.

The calculated SBS reflectivities reproduce the experimental scaling with SSD bandwidth. Moreover, we observe agreement with the measured absolute reflectivities when applying a non-linear damping on the ion acoustic waves. This model is based on the assumption of secondary ion acoustic decay observed in simulations[14]. In addition, the observed SBS and SRS losses are reduced with PS. This finding is consistent with experiments using lower intensity, low frequency laser beams[15], and with the modeling of our experimental conditions verifying theoretical predictions of Refs.[9,16,17].

II. EXPERIMENT

The experiments have been performed at the Nova Laser Facility at the Lawrence Livermore National Laboratory[18]. Cylindrical hohlraums of 2.75 mm length and 0.8 mm radius (scale-1) have been used. On either side, five laser beams with a total energy of 27 kJ enter the hohlraum through laser entrance holes (LEH) that are covered with 0.35μm thick polyimide. The hohlraums have been heated with nine f/4 laser beams and one f/8 interaction beam. All beams had a shaped pulse of 2.4 ns duration (examples are shown in Ref.[25]) rising from a 0.7 TW foot to 1.7 TW peak power per beam (pulse shape no. 22: PS22) resulting in an averaged intensity of $I_0 = 2 \times 10^{15}$ W cm^{-2} at peak power in the LEH plane[19]. The f/8 interaction beam was smoothed with a Kinoform Phase Plate (KPP)[20] giving an intensity of $I_0 = 2 \times 10^{15}$W cm^{-2} or with a Random Phase Plate (RPP) with 9.1 mm square elements[21] producing a smaller focal spot to achieve $I_0 = 4 \times 10^{15}$W cm^{-2} in the LEH plane.

The RPPs and KPPs produce a uniform intensity envelope without large scale-length inhomogeneities but have fine scale hot spots (speckles) with intensities significantly higher than the averaged intensity. Provided the phase changes produced by the KPP or RPP cause a shorter transverse coherence length than those associated with the wave-front of the Nova laser (as they have been designed to be), these latter effects are unimportant. The KPP envelope is super-Gaussian and the mean intensity near the focus is well defined. The

RPP envelope has a Bessel function shape with a FWHM intensity and a peak intensity that differ by 50 %. Provided there are at least hundreds of speckles within an area over which the intensity of the envelope varies little, the speckle distribution for the RPP and KPP depend only on the local envelope intensity. Simulations indicate that for the hohlraum experiment most of the SBS and SRS reflectivity is related to the hot spots[17,22,23].

The laser focal spot is further smoothed through use of SSD and PS. With SSD, the combination of bandwidth of up to 0.15 nm at 351 nm together with a dispersive grating in the beam line serves to move the speckles in the focal plane on short time scales (coherence time = 12.3 ps/$\Delta\omega \sim 4$ ps for a laser bandwidth of $\Delta\omega = 0.3$ nm at 1ω). The bandwidth was critically dispersed (1 color cycle). For the experiments with PS, wedged birefringent crystals were installed between the KDP frequency conversion crystals and the focus lens (cf. Fig. 1) resulting in two orthogonally polarized sets of laser speckles in the target plane spatially separated by 30μm and efficiently reducing the fraction of the beam with intensities far above the average intensity[9].

Figure 1 shows a schematic of the scattering detectors for SBS and SRS from the f/8 laser beam. Backscattering into the lens has been measured with a full aperture backscattering diagnostic (FABS)[5]. The system observes the bakscattered light through the last turning mirror for the incoming beam and images the light onto a spectralon^{TM} plate. The re-emission from the plate has been measured with diodes and also coupled into optical fibers for temporally and spectrally resolved detection with optical streak cameras. We have absolutely calibrated the whole detection system *in situ* by auto-reflecting 8 % of a full-power laser shot into the detector. Light scattered at larger angles up to 22° has been detected with a near backscattering imager (NBI)[24] consisting of a calibrated aluminum scatter plate mounted around the lens and two-dimensional imaging detectors for SBS and SRS. The latter shows that the near backscattering contribution to the overall reflectivity is small of order 10-20 % because the measurements in this study have all been applying random phase plate beam smoothing. Scattering at large angles (> 15 %) is negligible (see also Fig. 5 of Ref.[25])

III. RESULTS AND COMPARISON WITH SIMULATIONS

Figure 2 shows experimental SBS and SRS time integrated scattering data as a function of the laser bandwidth. The bandwidth and power of the f/8 laser beam has been measured at 1ω as well as at 3ω using a full aperture sample of a focus lens reflection. We find that the pulse shapes were reproducible to within 15 % rms. The f/8 experiments give almost a factor of 2 higher SBS reflectivities than experiments at f/4 (obtained with a 3 GHz frequency modulator) and comparable SRS values for zero laser bandwidth. With increasing laser bandwidth we find that the time integrated SBS reflectivity reduces from $5-6$ % at 0 nm bandwidth to $0.6-1$ % for a 3ω bandwidth > 0.1 nm. The SRS reflectivity shows a factor of 2-4 reduction. The error bar for each data point is estimated to be 20 %. Moreover, we observe that PS further reduces SBS losses by 20 % without showing a beneficial effect for SRS at this intensity. At high intensities [cf. Fig 2(b)], the total SBS reflectivity is larger by about a factor of 2 (no SSD) and shows the same reduction of a factor of 5 for a 3ω bandwidth of 0.1 nm as the data at 2×10^{15} W cm^{-2}. In this case, the effect of PS is very large: PS reduces the SBS and SRS reflectivity by a factor of 5 to below the 1 % level.

Calculations of the SBS and SRS reflectivity are sensitive to a number of plasma and laser parameters, in particular to the electron temperature and density, the flow velocity and density gradient scale length, laser intensity and laser wavelength. Therefore, calculations of hohlraum reflectivities require elaborate simulations of plasma conditions and modeling of the SBS and SRS process. First, 2-D radiation-hydrodynamic calculations of the hohlraum plasma conditions with the code LASNEX[6,26,27] provide temperature, density, and plasma flow data. The calculations use the measured absorbed laser power rather than the actual incident power to account for the effect of the stimulated scattering losses on the plasma parameters. An integrated test of the results, to be used below to calculate reflectivities with F3D, is obtained by using the simulated plasma parameters to calculate the spatial gain profile of SBS and SRS using linear convective gain theory. The gain profiles indicate that SBS grows primarily in the Au blow-off plasma with a peak amplitude gain of 10 when

the maximum laser intensity of 2×10^{15}W cm^{-2} is reached at $t = 1.5$ ns. The calculations further show that SRS primarily grows in the low$-Z$ plasma with an amplitude gain of 5.

Figure 3 shows experimental SBS and SRS spectra together with the calculated gain values versus wavelength and time. In particular, the wavelength of the SBS signal is sensitive to the plasma flow as well as to the temperature via the dispersion relation for ion acoustic waves. With exception of the early time signal at $t < 0.3$ ns which is due to light scattering from the exploding membrane that has confined the gas, the comparison of the wavelength and relative intensity of the scattered signal with the wavelength and absolute calculated value of the gain shows good agreement. In particular for the case with 0.1 nm SSD the experimental wavelength shift away from the incident laser wavelength λ_0 is 0.2 nm while the calculated shift is 0.1 nm. This implies that the sum of the sound speed in the Au plasma and its blow-off velocity is calculated to within $\sim 10\%$. In addition, the measured and the calculated spectra peak at maximum laser intensity at 1.5 ns.

The SRS spectra are not as well understood. The wavelength of the SRS signal is sensitive to the electron density and to the electron temperature via the Bohm-Gross dispersion relation. The calculated gain peaks when the observed SRS peaks at 1 ns which is 0.5 ns before peak power. While the results in the Au plasma are not altered if we use LASNEX modeling with magnetic fields[27], the calculated SRS spectra reproduce the peak at 1 ns *only* when we include magnetic fields. The SRS gain exponent is modest (< 5) and peaks at 1ns because, with B-fields, the electron temperature and thus the Landau damping of the Langmuir wave, increases rapidly as the power ramps up to its peak at $t = 1.5$ ns. The observed SRS spectrum is broadened towards shorter wavelengths compared to the linear gain calculation. This observation might be interpreted as filamentation of the laser beam in the low$-Z$ plasma close to the laser entrance holes. However the calculated gain for filamentation in this region is only sufficient to focus the most intense speckles. Improved diagnostics of filamentation will be required to better understand the SRS spectra from hohlraums.

Because the calculated gain for the average intensity is not large, one can reasonably

assume that SBS originates in space and time where the linear gain is maximum, particularly since LIP calculations agree with the history of the SBS spectral shift. To calculate the reflectivity, we use F3D which includes the laser self-focusing and speckle statistics. Figure 4 shows the comparison between the experimental peak SBS reflectivity and F3D simulations of the SBS reflectivity for $I_0 = 2 \times 10^{15}$W cm^{-2} (a) and for $I_0 = 4 \times 10^{15}$W cm^{-2} (b). The cylindrical symmetric 2-D LASNEX calculations model case (a) better than the higher intensity case (b) because in (a) the intensity is the same as those of the other nine heater beams. The simulations are 120 ps long (enough to reach steady-state conditions) using a box of $56 \times 56 \times 88 \mu$m^3. The experiment is modeled at the time of peak SBS, i.e at $t = 1.5$ ns. Linear SBS gain calculations along LASNEX hydrodynamic profiles show that the SBS growth is localized in the Au-plasma blow-off (with a calculated averaged ionization state $< Z >= 52$). The length of the simulation box is chosen so as to contain the amplification region that gives the maximum linear gain. This can be seen from the fact that LIP SBS gain calculations of this box give the same maximum gain as the whole Au blow-off while SBS from regions outside of the simulation box is non-resonnant with SBS that grows inside of it. The averaged electron and ion temperatures are $T_e = 2.5$ keV, $T_i = 1.7$ keV[28]. The electron density (divided by the critical density) increases linearly from 0.165 to 0.2, and the fluid velocity linearly increases from -1.83×10^7 cm s^{-1} to -1.8×10^7 cm s^{-1}. Finally, the average laser intensity imposed at the left boundary of the simulation region is 7×10^{14}W cm^{-2}, accounting for absorption along the beam path inside the hohlraum (this for an intensity of 2×10^{15}W cm^{-2} in vacuum at best focus). We find that calculations with linearly damped ion acoustic waves describe the dependence of SBS on SSD and PS although the absolute reflectivities are larger by a factor of $2 - 10$ than the experimental data. We attribute this difference to non-linear saturation processes such as ion acoustic decay[14] or ion trapping[29].

To account for saturation processes, we include a non-linear ion wave damping, γ_i, of the form $\gamma_i = \gamma_L + \omega_{ac} (\delta n_e / \delta n_{thres})^4$. Here, γ_L denotes Landau damping and δn_{thres} is the threshold fluctuation for ion acoustic decay (IAD). The form of the damping approximates a smoothed Heaviside function around threshold which simplifies the numerical modeling.

The rather large value for the damping, which prevents growth above threshold, is motivated by the experimental observation (see Fig. 2) that the reflectivity increases slowly with laser intensity. In the modeling, non-linear damping sets in when the ion acoustic wave amplitude δn_e reaches about 10-20 % of its theoretical threshold for ion acoustic decay[14]. Saturating the ion wave amplitude below the IAD threshold is in fact consistent with the kinetic simulations which show this behavior after the initial depletion of the wave by IAD. By adjusting the ion wave amplitude in this way, we find that the absolute calculated SBS reflectivity and the scaling with SSD agrees with the experimental peak reflectivity without further assumptions. The absolute reflectivities for PS agree less well at this intensity.

For the conditions of the experiment, the F3D modeling shows that SBS is generated mostly (~ 75 %) in the laser speckles with intensities of $(2-4) \times I_0$. SSD is most effective in reducing the life time of the speckles in the high$-Z$ wall plasma so that SBS from the speckles does not reach the saturated steady-state regime. The modeling shows that > 70 ps is needed to achieve a saturated acoustic wave amplitude over the length of a speckle, $\sim 180\mu$m, which is much longer than the correlation time for SSD in these experiments ($\tau = 2\pi/\Delta\omega \approx 4$ ps). In the saturated state, ion acoustic waves exist at an enhanced level just below the threshold of non-linear damping. The SBS reflectivity scales with the hotspot lifetime, the laser coherence time, as long as that time is shorter than the time required to reach steady state inside a hotspot from the enhanced level of fluctuations. Polarization smoothing reduces the number of high intensity speckles (with $I \geq 3I_0$) instantaneously and increases the fraction of the laser power at the mean intensity. As a result the average power located in the hotspots contributing to the reflectivity and average ion acoustic wave fluctuation amplitude are reduced. The calculations show that SSD also reduces filamentation and in this way further contributing to a reduced SBS reflectivity. However, filamentation in the Au plasma is not the dominant mechanism leading to SBS. This result is consistent with the blue shift of the SBS signal (Fig. 3) for SSD. Filamentation would cause an increased blue shift[5] because SBS would occur further away from the hohlraum wall where expansion velocities are larger. Moreover, the small dependence of the reflectivity on the laser f-number

as shown in Fig. 2(a) further indicates that filamentation is not dominant (F3D simulations reproduce the factor of two reduction in going from f/8 to f/4).

To model the laser interaction with the gold plasma, we also included the effect on the laser beam of propagating through about 1 mm of the gas plasma. At 2×10^{15}W cm^{-2}, the assumption of vacuum propagation is reasonable provided absorption is accounted for. However, at 4×10^{15}W cm^{-2}, the laser beam acquires temporal incoherence because of forward Brillouin scatter with an induced bandwidth equivalent to ~ 0.3 nm at 1ω. With this induced bandwidth added to the SSD bandwidth, modeling of the higher intensity SBS improved the agreement between the modeling and the experiment. In this case, the need for non-linear damping is more obvious since the simulations show no reduction of SBS with bandwidth for linear damping alone. The calculated reduction of SBS is consistent with the experiment when applying the non-linear model.

IV. CONCLUSIONS AND OUTLOOK

In summary, we have demonstrated that laser beam smoothing by SSD and PS very effectively controls laser backscattering in indirect drive ICF plasmas. For these gas-filled hohlraum experiments where the plasma and laser beam conditions approach those of future ICF experiments, we find that the smoothing techniques have reduced scattering losses to the 1 % level for high laser intensities. These findings may indicate additional margin to achieve ignition on future laser facilities such as the NIF. We further find that the scaling of the measured SBS reflectivity with SSD laser bandwidth and with PS is consistent with F3D modeling. Calculating absolute SBS reflectivities will require better understanding of non-linear ion wave processes in laser fusion plasmas.

ACKNOWLEDGMENTS

The authors would like to thank the Nova crew for technical support and P. E. Young

and J. E. Rothenberg for discussions. This work was performed under the auspices of the U.S. Department of Energy by the Lawrence Livermore National Laboratory under contract No. W-7405-ENG-48.

REFERENCES

1. J. F. Drake, P. K. Kaw, Y. C. Lee, et al.*et al.* Phys. Fluids **17**, 778 (1974). M. N. Rosenbluth, R. B. White, and C. S. Liu, Phys. Rev. Lett. **31**, 1190 (1973). D. W. Forslund, J. M. Kindel, and E. L. Lindman, Phys. Fluids **18**, 1002 (1975). M. N. Rosenbluth, Phys. Rev. Lett. **29**, 565 (1972).

2. W. L. Kruer, *The Physics of Laser Plasma Interactions* (Addison-Wesley, New York, 1988).

3. H. A.Baldis, E. M. Campbell, and W. L. Kruer, in *Physics of Laser Plasma*, edited by A. Rubenchik, and S. Witkowski (North-Holland, Amsterdam, 1991), pp. 361.

4. W. Seka, R. E. Bahr, R. W. Short, A. Simon, R. S. Craxton, D. S. Montgomery, and A. E. Rubenchik, Phys. Fluids B **4**, 2232 (1992).

5. B. J. MacGowan, B. B. Afeyan, C. A. Back *et al.*, Phys. Plasmas **3**, 2029 (1996).

6. L. J. Suter, R. L. Kauffman, C. B. Darrow *et al.*, Phys. Rev. Lett. **73**, 2328 (1994). Phys. Plasmas **3**, 2057 (1996).

7. S. Skupsky, R. W. Short, T. Kessler, R. S. Craxton, S. Letzring, and J. M. Soures, J. Appl. Phys. **66**, 3456 (1989).

8. J. E. Rothenberg, J. Appl. Phys. **87**, 3654 (2000).

9. E. Lefebvre, R. L. Berger, A. B. Langdon, B. J. MacGowan, J. E. Rothenberg, and E. A. Williams, Phys. Plasmas **5**, 2701 (1998).

10. T. R. Boehly, V. A. Smalyuk, D. D. Meyerhofer, J. P. Knauer, D. K. Bradley, R. S. Craxton, M. J. Guardalben, S. Skrupsky, and T. J. Kessler, J. Appl. Phys. **85**, 3444 (1999).

11. S. H. Glenzer, L. J. Suter, R. E. Turner *et al.*, Phys. Rev. Lett. **80**, 2845 (1998).

12. R. L. Berger, E. A. Williams, A. Simon, Phys. Fluids B **1**, 414 (1989).

13. R. L. Berger, C. H. Still, E. A. Williams, and A. B. Langdon, Phys. Plasmas **5**, 4337 (1998).

14. B. I. Cohen, B. F. Lasinski, A. B. Langdon, and E. A Williams, Phys. Plasmas **4**, 956 (1997).

15. J. Fuchs, C. Labaune, S. Depierreux, H. A. Baldis, and A. Michard, Phys. Rev. Lett. **84**, 3089 (2000).

16. S. Hüller, Ph. Mounaix, and V. T. Tikhonchuk, Phys. Plasmas **5**, 2706 (1998); **5**, 3794 (1998)

17. R. L. Berger, E. Lefebvre, A. B. Langdon, J. E. Rothenberg, C. H. Still, and E. A. Williams, Phys. Plasmas **6**, 1043 (1999).

18. E. M. Campbell, J. T. Hunt, E. S. Bliss, D. R. Speck, and R. P. Drake, Laser Part. Beams **9**, 209 (1991).

19. Because the grating delay time was ~ 60 ps in these experiments the laser pulse shape was unaffected by SSD unlike the previous 3 GHz with a 350ps delay.

20. S. N. Dixit, M. D. Feit, M. D. Perry, and H. T. Powell, Optics Lett. **21**, 1715 (1996).

21. Y. Kato, K. Mima, N. Miyanaga, S. Arinaga, Y. Kitagawa, M. Nakatsuka, and C. Yamanaka, Phys. Rev. Lett. **53**, 1057 (1985).

22. M. R. Amin, C. E. Capjack, P. Frycz, W. Rozmus, and V. T. Tikhonchuk, Phys. Rev. Lett. **71**, 81 (1993).

23. Ph. Mounaix, L. Divol, S. Hüller, and V. T. Tikhonchuk, Phys. Rev. Lett. **85**, 1057 (4526).

24. R. K. Kirkwood, C. A. Back, M. A. Blain, D. E. Desenne, A. G. Duliu, S. H. Glenzer, B. J. MacGowan, D. S. Montgomery, and J. D. Moody, Rev. Sci. Instrum. **68**, 636 (1997).

25. S. H. Glenzer, L. J. Suter, R. L. Berger *et al.*, Phys. Plasmas **7**, 2585 (2000).

26. G. B. Zimmerman and W. L. Kruer, Comments Plasma Phys. Controlled Fusion **2**, 85 (1975).

27. S. H. Glenzer, W. E. Alley, K. G. Estabrook *et al.*, Phys. Plasmas **6**, 2117 (1999).

28. These calculated parameters have recently been verified with Thomson scattering and x-ray spectroscopic measurements.

29. D. W. Forslund, J. M. Kindel, and E. L. Lindman, Phys. Fluids **18**, 1017 (1975). H. X. Vu, K. Y. Sanbonmatsu, B. Bezzerides, and D. F. DuBois, Phys. Rev. Lett. **82**, 932 (1999). C. E. Clayton, C. Joshi, and F. F. Chen, Phys. Rev. Lett. **51**, 1656 (1983).

FIGURES

Fig. 1. Schematic of the hohlraum experiment showing the detectors for SBS and SRS measurements.

Fig. 2. Time-integrated SBS and SRS reflectivity from gas-filled hohlraums measured with an f/8 (or f/4) interaction beam at 2×10^{15} W cm^{-2} (a) and at 4×10^{15} W cm^{-2} (b). All data points were taken with phase plates. The typical error is $\sim 20\%$. The dashed curve is a guide through each set of data for SBS and SRS.

Fig. 3. Temporally resolved SBS spectra from experiments with laser intensities of 2×10^{15} W cm^{-2} without SSD (a), with 0.1 nm SSD (b), and from gain calculations (c). Same for SRS (d)-(f). The gray scale indicates the relative intensity on the experimental spectra [(a), (b), (d), and (e)] and to absolute gain on the calculated spectra [(c) and (f)].

Fig. 4. Comparison of peak SBS reflectivity with F3D calculations (shown as straight lines) for the experiments with 2×10^{15} W cm^{-2} (a) and 4×10^{15} W cm^{-2} (b).

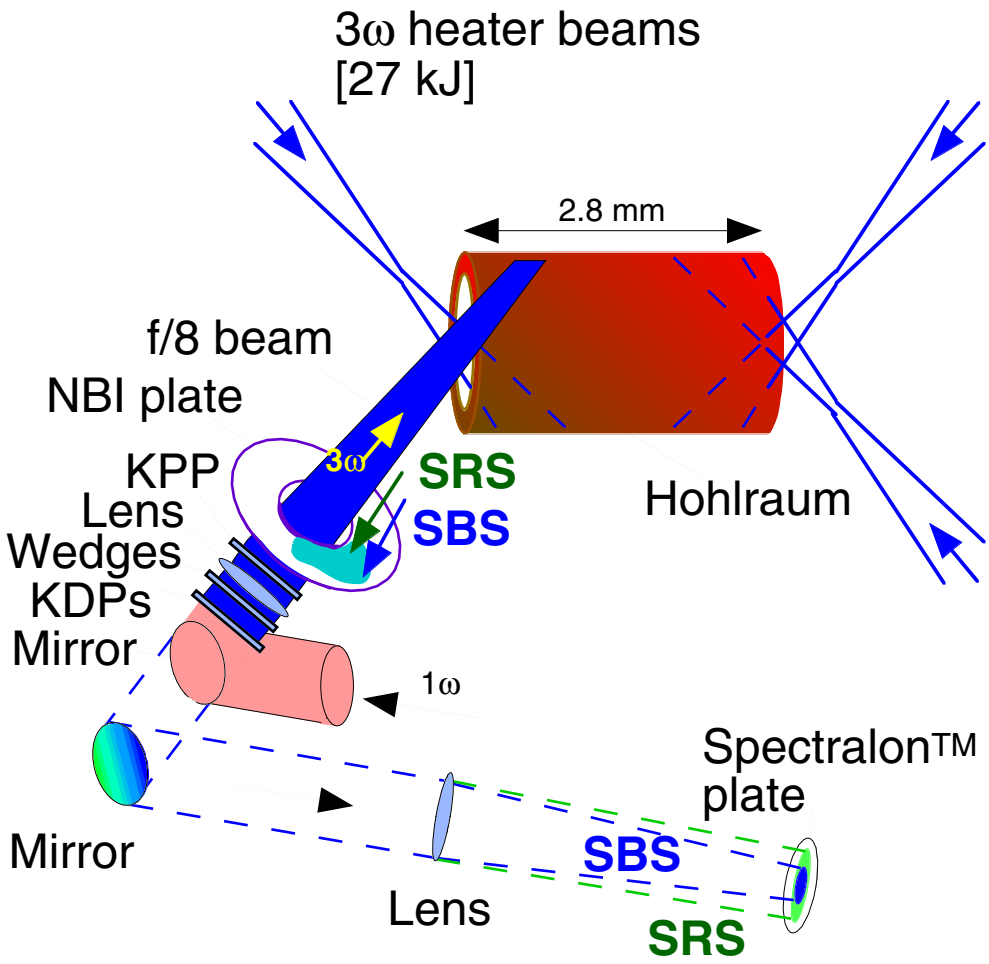
3ω heater beams
[27 kJ]
2.8 mm
f/8 beam
NBI plate
KPP
Lens
Wedges
KDPs
Mirror
3ω
SRS
SBS
Hohlraum
1ω
Spectralon™
plate
Mirror
Lens
SBS
SRS

Figure 1

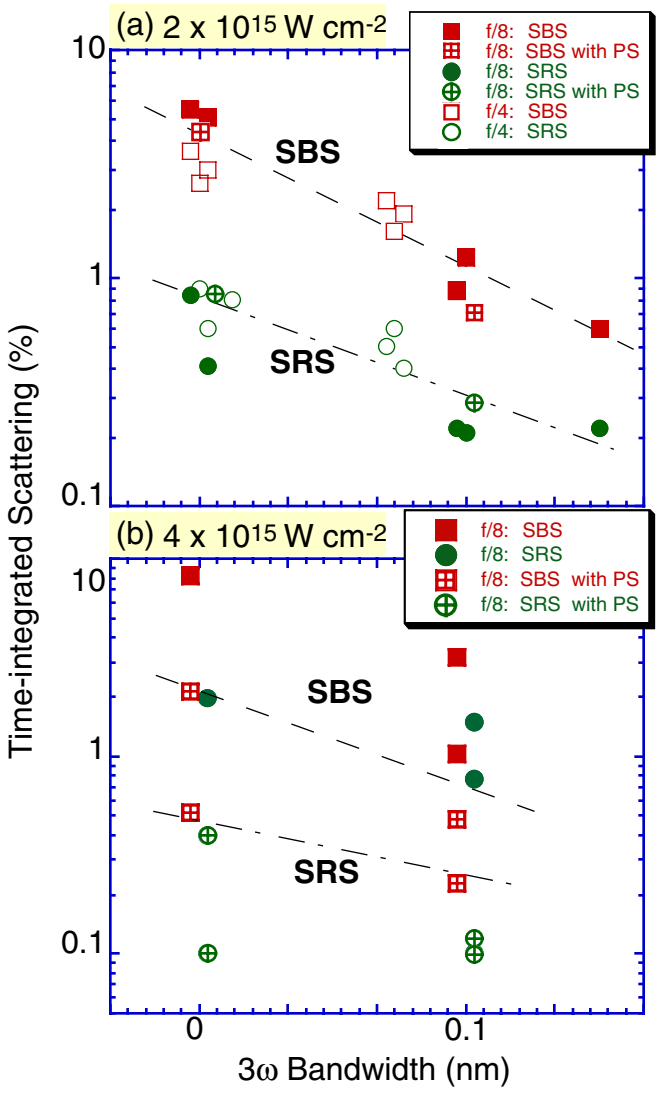
(a) 2 x 10^15 W cm^-2
f/8: SBS
f/8: SBS with PS
f/8: SRS
f/8: SRS with PS
f/4: SBS
f/4: SRS
SBS
SRS
(b) 4 x 10^15 W cm^-2
f/8: SBS
f/8: SRS
f/8: SBS with PS
f/8: SRS with PS
SBS
SRS
Time-integrated Scattering (%)
10
1
0.1
0
0.1
3ω Bandwidth (nm)

Figure 2

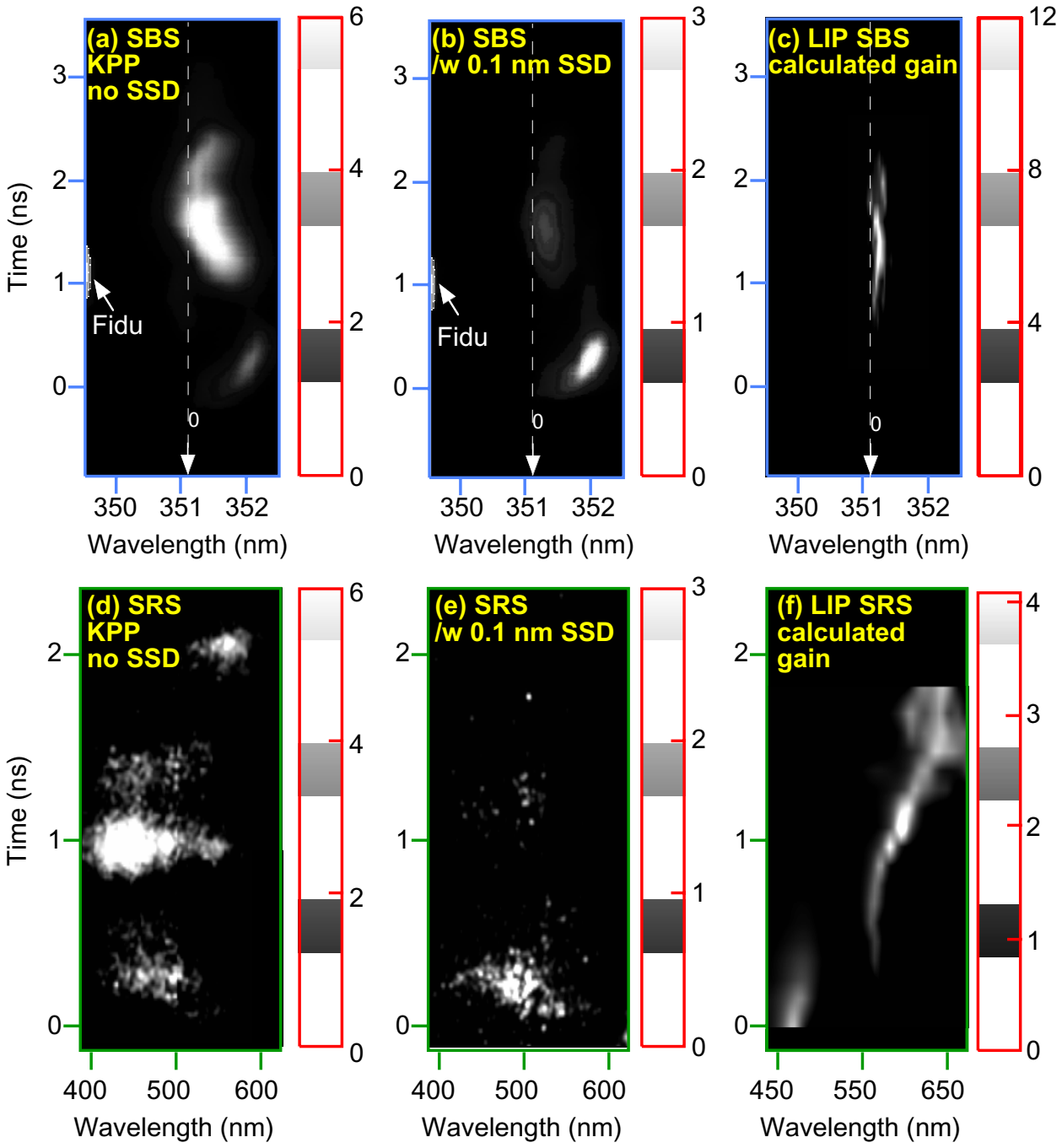
(a) SBS
KPP
no SSD
(b) SBS
/w 0.1 nm SSD
(c) LIP SBS
calculated gain
(d) SRS
KPP
no SSD
(e) SRS
/w 0.1 nm SSD
(f) LIP SRS
calculated
gain
Fidu
Time (ns)
Wavelength (nm)
350 351 352
400 500 600
450 550 650

Figure 3

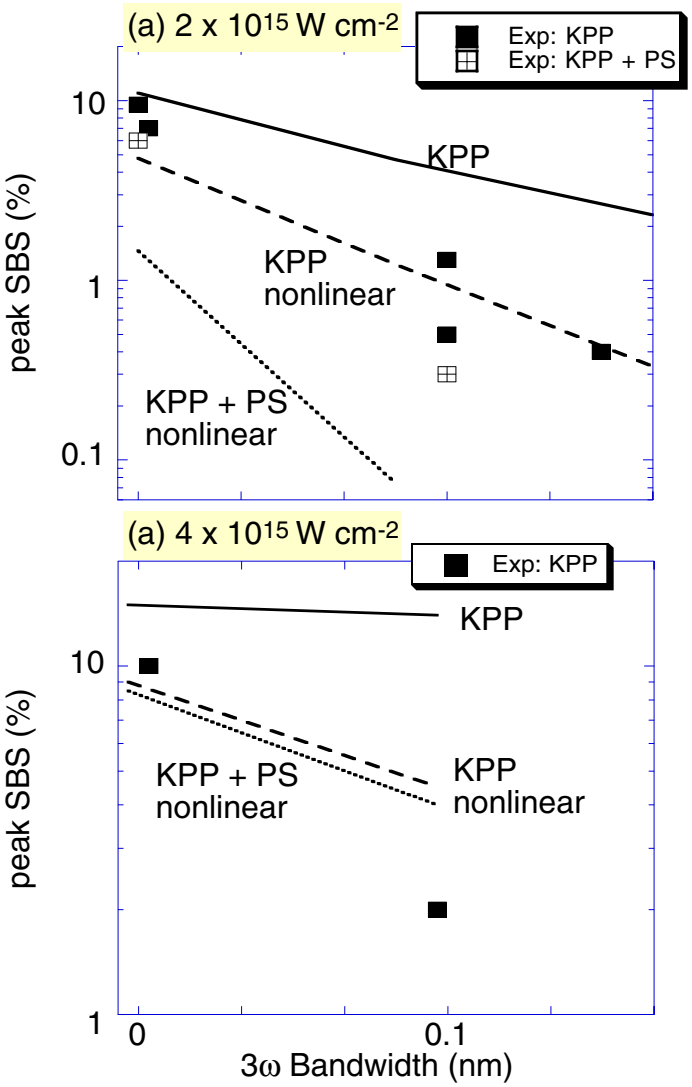
(a) 2 x 10^15 W cm^-2
Exp: KPP
Exp: KPP + PS
KPP
KPP
nonlinear
KPP + PS
nonlinear
peak SBS (%)
10
1
0.1
(a) 4 x 10^15 W cm^-2
Exp: KPP
KPP
KPP + PS
nonlinear
KPP
nonlinear
peak SBS (%)
10
1
0
0.1
3ω Bandwidth (nm)

Figure 4